Lei Xing, Qian Xu, Jiajia Zhu, Yongjiu Zhao, Saqer Alja'afreh, Chaoyun Song, and Yi Huang

A High-Efficiency Wideband Frequency-Reconfigurable Water Antenna With a Liquid Control System

Usage for VHF and UHF applications.

A distilled water dielectric resonator antenna (DRA) with a wide frequency-tuning range and high efficiency is presented in this article. It consists of a water resonator and a ground plane with a wideband bowtie feeding slot. The water resonator, having tunable dimensions, is employed to achieve frequency-reconfigurable characteristics. Mechanical switches and a microfluid pump are integrated to control the tuning process. The water DRA, with and without the liquid control system, is designed with a simulation tool and then fabricated and measured to validate the antenna's performance. It is demonstrated that the antenna exhibits high total efficiency (> 80%) across a wide frequency-tuning range from 168 to 474 MHz (for S_{11}, −10 dB) with a very compact volume of $278 \times 278 \times 131$ mm^3 ($0.155\lambda \times 0.155\lambda \times 0.073\lambda$ at 168 MHz). Compared with traditional reconfigurable antennas, this design provides a wider frequency-tuning range, a more compact size, and a higher degree of design freedom. It is therefore a promising candidate for very high-frequency (VHF) and ultrahigh-frequency (UHF) applications.

Digital Object Identifier 10.1109/MAP.2019.2946556
Date of current version: 6 November 2019

INTRODUCTION

Liquid antennas are a special type of antenna, in that they utilize fluid to transmit and receive radio signals. They have attractive features, such as reconfigurability, flexibility, stretchability, and possibly, a small radar cross section. Two kinds of liquid antennas have been investigated: liquid metal antennas [1], [2] and water-based liquid antennas [3]–[11]. As liquid metal antennas have a complicated fabrication process and a relatively high cost, water-based liquid antennas are normally preferred, and some relevant work has been reported [3]–[12]. Designs include distilled water antennas (e.g., a cylindrical water DRA [3], a transparent water patch antenna [4], a pure-water Yagi antenna [5]), saltwater designs (e.g., a monopole water antenna [6], a metal-loaded sea water antenna [7]), hybrid water antenna designs (e.g., an F-shaped monopole feed hybrid water antenna [8], both salt and

distilled water hybrid antennas [9]), and water-loaded antenna designs (e.g., a compact, water-loaded antenna [10], a high-efficiency water-loaded dipole antenna [11], and a high-gain water-based microstrip antenna [12]). These investigations have shown that water-based liquid antennas are versatile, efficient, and flexible; they could be promising candidates for maritime wireless communications, biological implantable antennas, and conformal antennas. Water-based liquids are easily accessible and low cost, but they suffer from low temperature limitations. Ionic liquid materials with a much wider fluid temperature range (from –60 to +200 °C) have been identified and used for antenna designs, but they are not widely available [13], [14].

Among existing water antennas, increased attention has been paid to reconfigurable designs. Compared to traditional reconfigurable antennas, the liquidity of water brings unique opportunities for antennas to achieve reconfigurability without the use of other active components. Some interesting designs have been reported, including a frequency-reconfigurable water DRA [15], a polarization-reconfigurable water DRA [16], a pattern-reconfigurable water-loaded multiple-input, multiple-output antenna [17], and a beamsteering, seawater-based reflect-array antenna [18]. All are different designs of reconfigurable water antennas.

Many current reconfigurable water antennas are configured manually, which limits the application of water antennas. Some designs introduce the use of the micropump to control the fluid, which improves the automation of water antennas [19]. However, for large-scale reconfigurable water antennas, the liquid control issue has not been fully solved; therefore, a control system with both electric and fluid control is desired.

In this article, a frequency-reconfigurable water antenna is proposed. The water DRA with and without a liquid control system is made and tested. A computer-controlled, liquid-reconfigurable system is introduced. A microfluid pump and mechanical switches are integrated into the system. Good results in terms of the frequency-tuning range, the antenna efficiency, and the realized gain are obtained. Compared to existing reconfigurable liquid antenna designs, the main features of the proposed design are that: 1) without using an external matching circuit, the operating frequency of the antenna can be continuously tuned from 168 to 474 MHz, which covers (partially) both VHF and UHF bands (the water loss is not significant across the working frequency band); 2) a high total efficiency of approximately 80–94.4% across the frequency band is achieved; 3) various working states are obtained in one structure; 4) a software-based liquid control system is developed, which controls the water flow effectively and efficiently in a general way.

ANTENNA CONFIGURATION AND DESIGN

WATER DRA CONFIGURATION

The geometry of the proposed antenna is displayed in Figure 1. It consists of a water resonator and a ground plane with a bowtie feeding slot. The water resonator is the main radiating element used to effectively transmit the energy from the feeding structure into the space. The bowtie slot etched on the ground plane is the feeding structure used to excite the water resonator mode. These two parts determine the antenna performance.

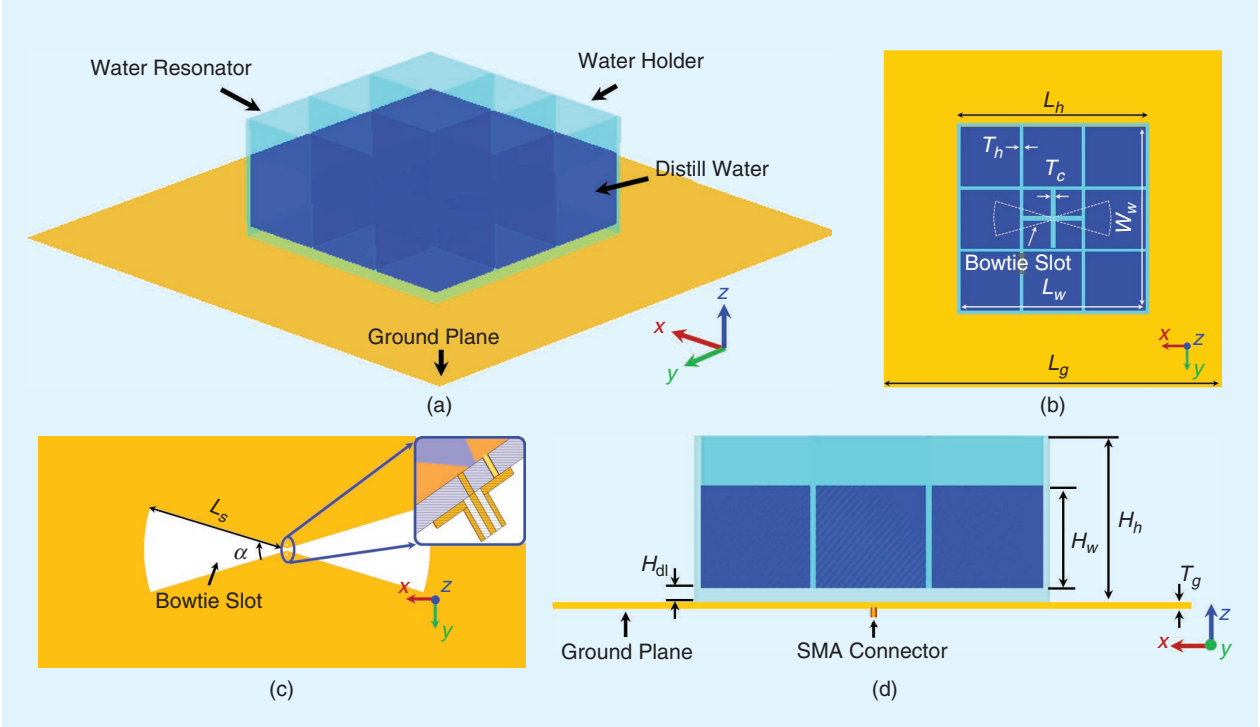

FIGURE 1. The geometry of the proposed antenna. (a) A perspective view, (b) the top view, (c) an enlarged view of the bowtie slot and the SMA connector connection, and (d) the front view.

The water resonator is formed by a hollow rectangular holder filled with distilled water. The holder has dimensions of $L_h \times L_h \times H_h$ and is divided into 3×3 cubic blocks by using transparent lattices with a thickness of T_h. The center block is further separated into four small blocks by embedding a center cross with a thickness of T_c (the center cross has a small gap with the bottom of the holder to promise four small water blocks with the same water level). The water resonator has dimensions of $L_w \times W_w \times H_w$. For different working states, L_w, W_w, and H_w will have different values. At the bottom of the water holder, a dielectric layer with a height of H_{dl} is used to isolate the water and the ground. The lattices, center cross, and dielectric layer work as low-permittivity dielectric inserts, and the material is acrylic plastic ($\varepsilon_r \approx 2.7 \sim 3$). Using low-permittivity inserts, the antenna can achieve a wide frequency-tuning range and high efficiency. The ground plane has dimensions of $L_g \times L_g \times T_g$, and the bowtie slot has a length of L_S and an angle of α. An SMA connector is coupled to the center of the slot to feed the antenna, as depicted in Figure 1(c).

THE WATER HEIGHT VARIATIONS AND WORKING FREQUENCY RANGE

For quick information, typical states with water height variations and related frequency-tuning range are summarized in Table S1. Note that the working states of the proposed design are not limited to the states listed; more working states can be obtained with different combinations of water blocks and various water heights.

TABLE S1. THE WATER HEIGHT VARIATIONS AND WORKING FREQUENCY RANGE OF THE TYPICAL STATES FOR THE PROPOSED DESIGN.

Typical States	Water Height Variations (mm)	Frequency-Tuning Range (MHz)
1	120–65	168–242
2	70–55	237–281
3	80–45	279–395
4	105–65	389–474

WATER DRA WITH A CONTROL SYSTEM

For a reconfigurable water antenna, how best to effectively and efficiently control the water over a wide frequency range is challenging (see "The Water Height Variations and Working Frequency Range). In previous studies, many reconfigurable water antennas were preconfigured or tuned manually, limiting the favorable characteristics of water antennas. To overcome this issue, a liquid control system is introduced to control the water conveniently and instantaneously without affecting the antenna's performance.

The control system consists of three parts: the electrical and fluid controls and the water DRA, as depicted in Figure 2. Acrylic connectors are fixed at the bottom of the water holder through the ground plane (nine connectors in this design, as shown in Figure 2), working as water inlets and outlets. Transparent water pipes are positioned underneath the ground plane to link the water DRA and valves, which also connect the fluid control part and the water DRA part.

The fluid control includes the valve's panel, water pump, and water reservoir. Before pumping the water into the holder, the distilled water is stored in the reservoir. When the pump is turned on, the distilled water is sucked from the reservoir and injected into the antenna through the acrylic connectors. During this process, the valve in and valve 1 to valve n are kept open, and the valve out is closed. When the water holder is filled to the desired level, the pump is turned off and all of the valves are kept closed. The distilled water can be drained when the valve in and valve 1 … n are closed and the valve out is open. By controlling the on and off states of the valves, various working states of the water DRA can be realized, resulting in a frequency reconfiguration in this proposed design.

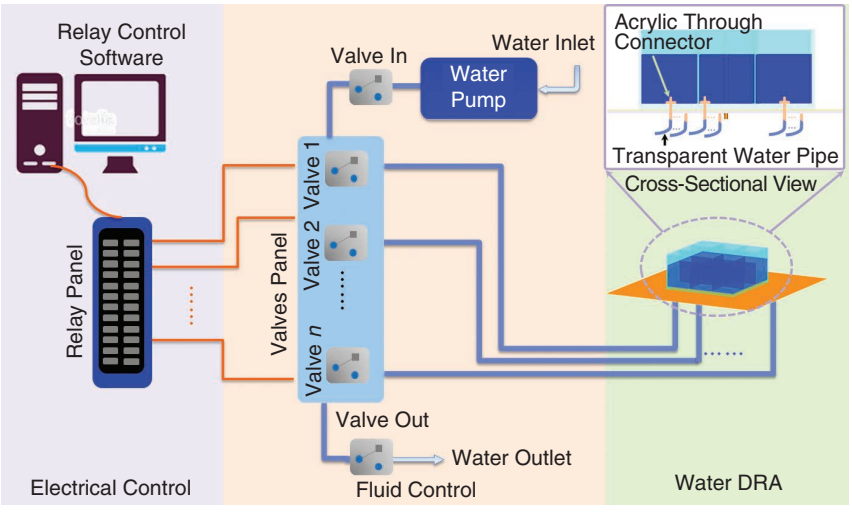

FIGURE 2. The water DRA electrical and fluid control system.

To avoid affecting the performance of the antenna, the water pump and valves as well as the transparent water pipes are expected to have a compact size, be lightweight, be cost-effective, and have low power consumption. In this design, a micropump with dimensions of $59 \times 24 \times 24$ mm^3 and a weight of 40 g is employed. It requires a 12-V dc voltage and has a flow rate from 240 to 400 mL/min. The speed of the flow rate can be adjusted by tuning the voltage applied. The minivalves have dimensions of $10 \times 29.5 \times 24.3$ mm^3 and a weight of 10 g. They can be arranged on the valves panel according to the specific antenna design, which is

valuable for the liquid control of large-scale water antennas and water antenna arrays.

The electrical control consists of a relay panel and real-time liquid control software. The relay panel has several sockets, and each socket is connected to one valve. The real-time liquid control software is developed in house to manage the relay panel and valves. In addition, the software can record the reflection coefficient and related parameters of the water DRA under different states.

ANTENNA OPERATION PRINCIPLE

The idea of the proposed design is to form water DRAs of diverse dimensions using a single device by filling the water holder to any desired level. Such flexibility is obviously convenient for liquid antennas but quite difficult for conventional solid DRAs. By using this strategy, both horizontal and vertical dimensions of the water DRA can be continuously and effectively tuned, offering a higher degree of design freedom compared to that of solid DRAs.

To explain the process clearly, four typical states are illustrated in Figure 3. For state 1, the water holder is fully filled with the distilled water. The water DRA has the largest dimension, consequently, the lowest resonant frequency of the TE_{11} mode. When the water height H_W decreases, the resonant frequency increases simultaneously. For states 2 and 3, specific water blocks are filled with water. Water DRAs with a higher resonant frequency (compared to state 1) can be obtained. For state 4, the center water block is excited and the water DRA has a much higher resonant frequency compared to the three previous states. Other states can also be employed. This design overcomes the drawbacks of solid DRAs and offers unique features of water's fluidity to reconfigure the antenna size conveniently.

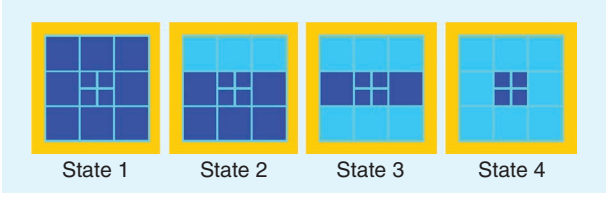

FIGURE 3. The typical working states of the water DRA.

For each state (states 1–4), the fundamental mode of the water DRA is excited. By using a combination of magnetic and dielectric waveguide models, as stated in [20], the lowest mode ($TE^{x}_{\delta 11}$ mode in this design) and its resonant frequency can be estimated by using (1) and (2) [21]:

$$k_x \tan(k_x L_w/2) = \sqrt{(\varepsilon_{\text{eff}} - 1)k_0^2 - k_x^2}, \quad (1)$$

$$k_x^2 + k_y^2 + k_z^2 = \varepsilon_{\text{eff}} k_0^2, \quad (2)$$

$$k_y = \frac{\pi}{W_w}, k_z = \frac{\pi}{2H_w}, \quad (3)$$

where k_y and k_z are the wavenumbers in y and z directions, respectively. k_0 denotes the free-space wavenumber, the x direction is the wave-propagating direction, and ε_{eff} is the water resonator's effective permittivity.

To verify the mode analysis of the reconfigurable water DRA, the electrical field (E-field) distributions of typical states are illustrated in Figure 4. It is noted that the E-field is mainly concentrated inside the water DRA and a half-$TE^{x}_{\delta 11}$ mode pattern (due to the ground plane) is clearly observed.

PARAMETRIC STUDY

The general behavior of this frequency-reconfigurable water DRA is influenced by a number of parameters, including the thickness of the center cross lattice (T_c), the height of the dielectric layer (H_{dl}), the slot angle and slot length (α, L_S), and the length of the square ground plane (L_g). To achieve optimal performance, a parametric study is carried out. In the parametric study, two cases (i.e., state 1 and $H_W = 120$ mm, and state 4 and $H_W = 70$ mm) are mainly considered, which represents the lower and the higher frequency bound of the working states.

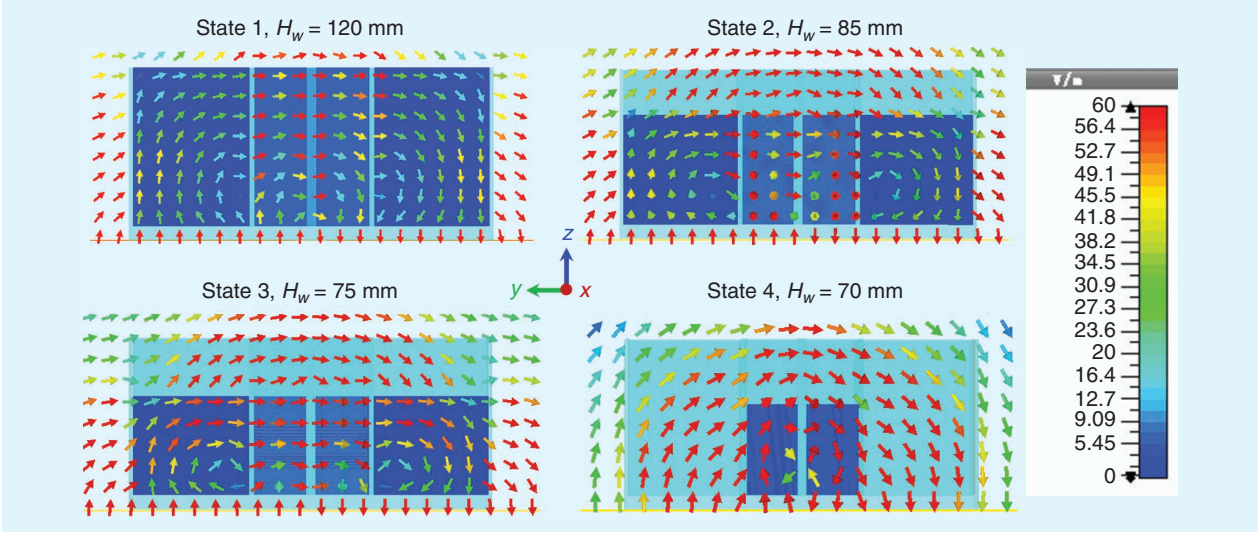

FIGURE 4. The E-field distributions of the $TE^{x}_{\delta 11}$ for the water DRA with typical working states.

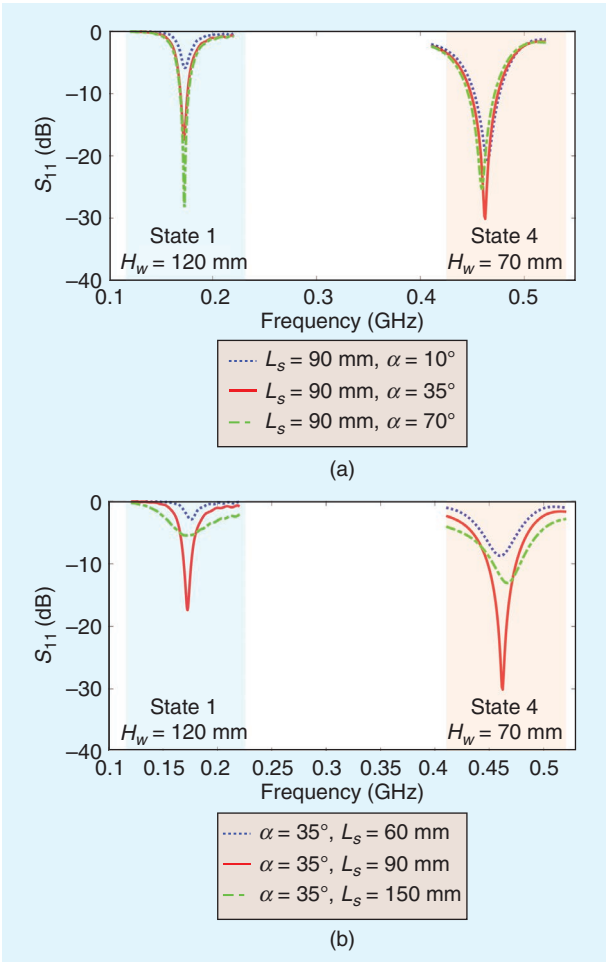

FIGURE 5. Simulated results with different values of L_S and α. (a) $L_S = 90$ mm and α varies. (b) $\alpha = 35°$ and L_S varies.

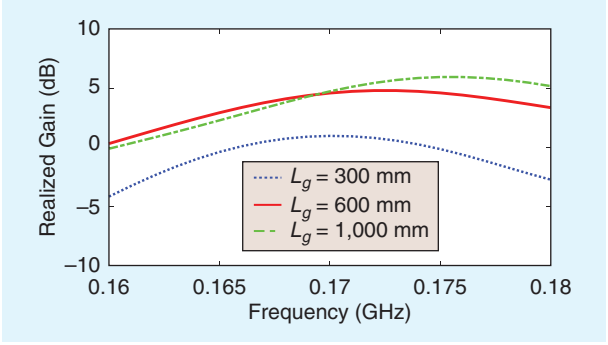

FIGURE 6. The simulated realized gains with different values of L_g.

EFFECT OF THE DIELECTRIC INSERT

The main idea behind adding dielectric inserts in the holder is to mix the high-permittivity material (distilled water) and low-permittivity material (the center cross and dielectric layer), forming a transparent water DRA. Both the loss and effective relative permittivity of the combined structure will be smaller than the resonator made by only distilled water. By using this principle, the proposed design can have high efficiency in all possible working states.

The center cross lattice with low permittivity is an important part and the value of T_c is critical, especially for state 4. If a thin center cross was used, a low working frequency would be obtained. At the same time, the loss of the combined DRA is increased; thus, the radiation efficiency would be reduced. A tradeoff between the lowest working frequency and the radiation efficiency must be considered. By choosing the center cross thickness properly, the optimal bandwidth and radiation efficiency for the target frequency band can be achieved when $T_c = 7$ mm.

The dielectric layer at the bottom of the holder can improve the matching of the antenna without using extra circuits, though some designs used this method to achieve a broad bandwidth [6]. The effects of the dielectric layer are similar to those of the center cross. With the increase of the dielectric layer height (H_{dl}), the working frequency shifts upward, the radiation efficiency as well as the bandwidth increases, at the expense of extending the antenna size. Thus, a tradeoff between the achievable bandwidth and the compact size has been considered by choosing $H_{dl} = 11$ mm mm in the final design.

EFFECT OF THE FEEDING SLOT

One major challenge of reconfigurable antennas with a wide tuning range is the wideband feeding structure design. In this article, a bowtie-shaped slot is chosen, which offers a smooth, gradual transition from the coaxial feed line to the radiating element. The slot size is crucial in providing a wideband response. A relatively small-size slot may impede the energy coupled to the antenna. If the slot is too large, the amount of radiation spilling beneath the ground plane increases, which affects the directivity of the antenna. Thus, well-designed slot dimensions are needed for all possible working states.

To study the effects of the feeding slot, the simulated S_{11} as a function of α and L_S are plotted in Figure 5. Two typical states are employed to illustrate the process. It is observed in Figure 5(a) that, as the value of α increases, the higher frequency bound S_{11} is stable, while the lower frequency-bound S_{11} is affected. When α is further increased from 35 to 70°, the S_{11} response does not change significantly; however, the directivity of the antenna will deteriorate as the radiation leaks under the ground plane. Thus, the slot angle $\alpha = 35°$ is preferred.

Three slot-length values of L_S, i.e., 60, 90, and 150 mm, are selected and the slot angle α is kept at 35°, as presented in Figure 5(b). It is noted that the slot length affects both the higher and lower bounds of the working frequency. Neither too-large nor too-small slot sizes are preferred. By choosing the proper values of α and L_S, the impedance matching can be improved. The optimal performance is acquired when $\alpha = 35°$ and $L_S = 90$ mm.

EFFECT OF THE GROUND PLANE SIZE

For a rectangular DRA mounted on an infinite ground plane (excited in the TE_{11} mode), the ground plane size may have an impact on the radiation patterns and influences the realized gain of the antenna, especially for low frequencies. For a given state (state 1 and $H_W = 120$ mm), the realized gain curves for different values of L_g are shown in Figure 6. It can be seen that, with the L_g value varied from 300 to 600 mm, the realized gain greatly increases from 0.78 to 4.78 dB. This is because the large-size ground plane

reduces the leakage of the radiated power to the lower half of the space and improves the realized gain. When L_g is further increased from 600 to 1,000 mm, the realized gain is stable; thus, for some space-limited applications, the $L_g = 600$ mm can be chosen to save more space.

ANTENNA FABRICATION AND MEASUREMENTS

To verify the design, a transparent water DRA with a wide frequency-tuning range was fabricated and measured; the prototype of the proposed design is displayed in Figure 7. The optimal parameters are $L_G = 600$ mm, $L_H = 278$ mm, $L_S = 90$ mm, $T_H = 4$ mm, $T_C = 7$ mm, $T_G = 1.6$ mm, $H_H = 131$ mm, $H_{\mathrm{DL}} = 11$ mm, and $\alpha = 35°$. Distilled water was used in the measurement, and the relative permittivity and loss tangent of the distilled water at room temperature (25 °C) can be found in Figure 8, which was measured using Agilent Dielectric Probe 85070. The results were compared with Computer Simulation Technology's (CST's) Debye model and a very good agreement was obtained.

The antenna performances are evaluated in terms of the S_{11}, total efficiency, radiation pattern, and realized gain. Figure 9 depicts the simulated and measured S_{11} of selected states. For all of the demonstrated states, the measured results agree well with the simulated ones. The frequency-tuning ability of the proposed design is demonstrated and various tuning states with diverse combinations of water blocks and water heights are investigated. For a specific state, the resonant frequency of the water DRA increases as the water height decreases. By considering all of the possible states and corresponding water heights, the working frequency of the proposed design can be continuously tuned from 168 to 474 MHz with reconfigurable water resonator dimensions from $270 \times 270 \times 120$ mm^3 to $87 \times 87 \times 65$ mm^3.

For water antenna designs, their efficiency is of great interest to researchers. The simulated total efficiency of possible working states is displayed in Figure 10 and the envelope is outlined,

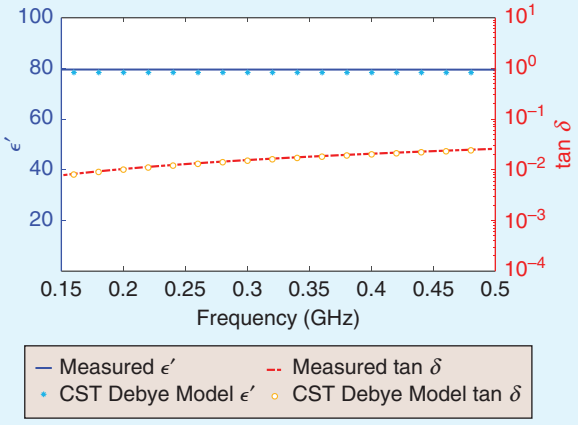

FIGURE 8. The relative permittivity and loss tangent of distilled water at 25 °C from the measurement and CST's Debye model.

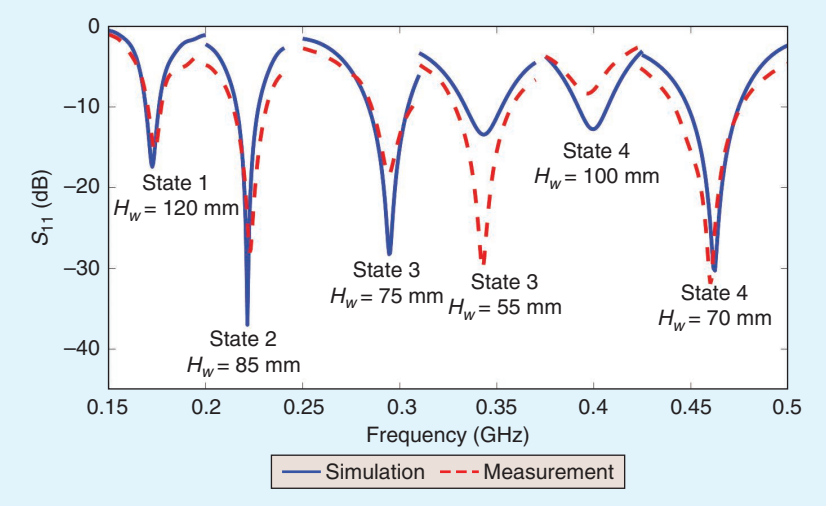

FIGURE 9. The simulated and measured S_{11} of the proposed water DRA.

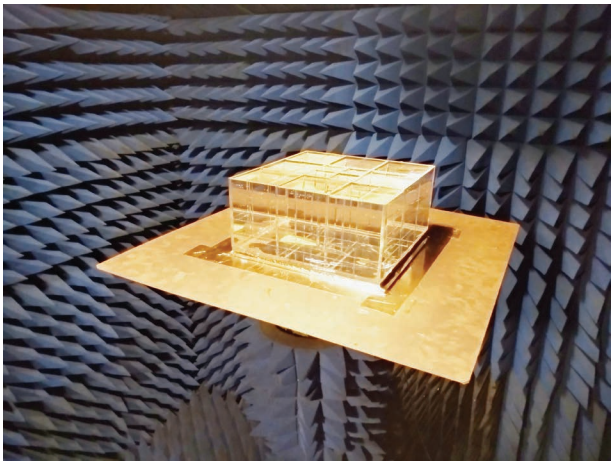

FIGURE 7. The water DRA prototype.

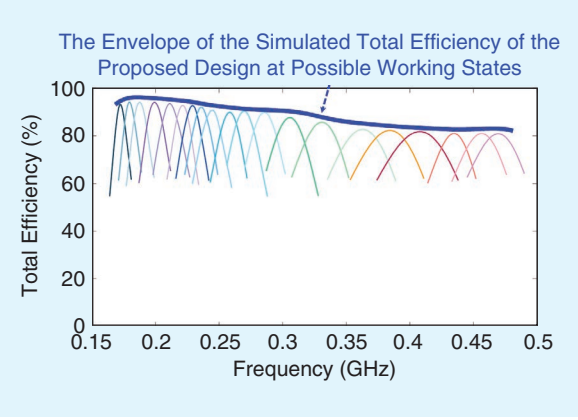

FIGURE 10. The simulated total efficiency of the proposed water DRA.

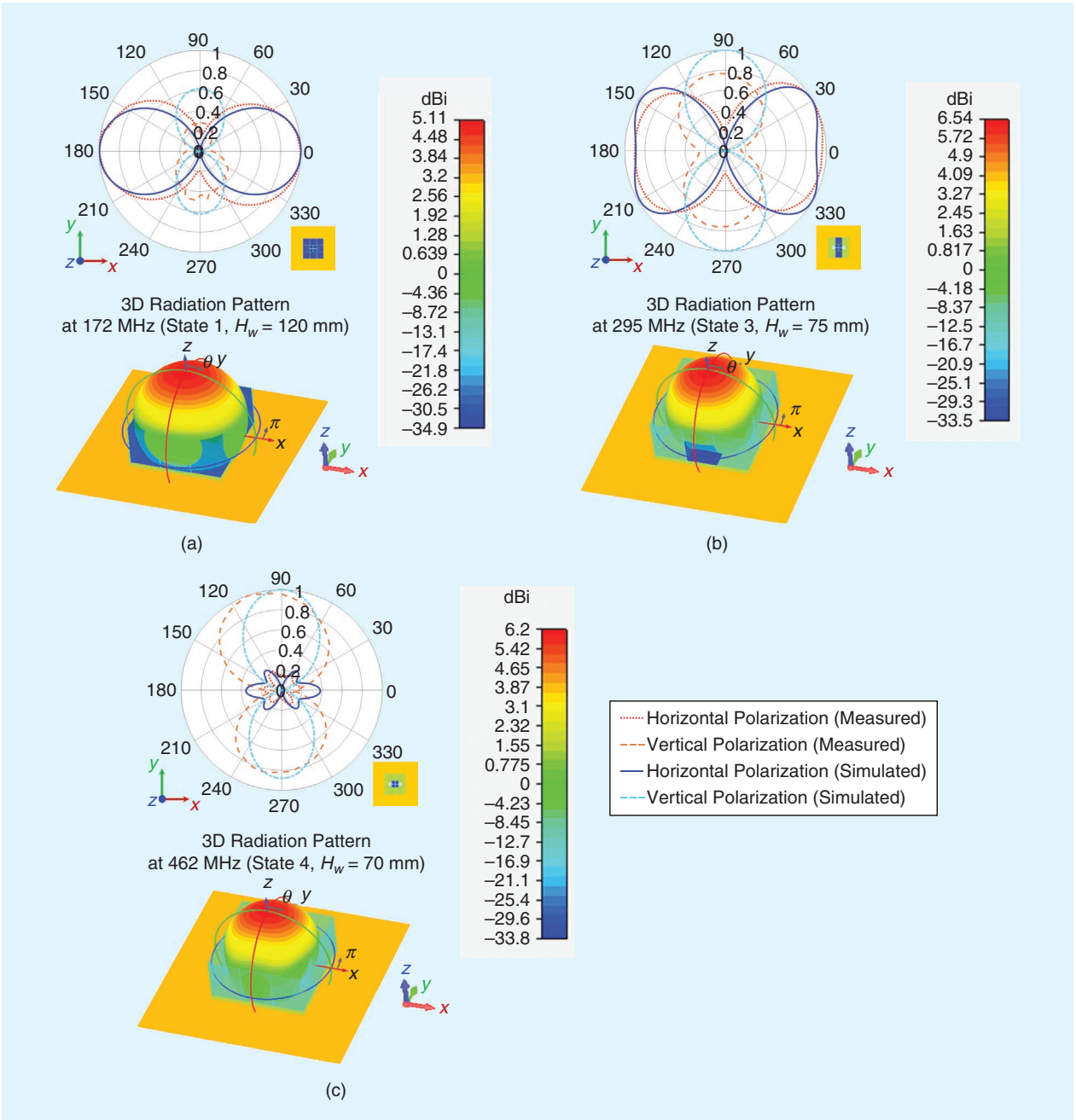

FIGURE 11. The simulated (2D and 3D) and measured (2D) radiation patterns in the *xoy* plane of the proposed antenna. (a) 172, (b) 295, and (c) 462 MHz.

which reflects the radiation ability and impedance matching of the proposed design. From the results, we can see that the simulated total efficiency is higher than 80% across the required band, which is better than most of the existing water antennas.

The radiation pattern and realized gain were measured in an anechoic chamber. The simulated and measured results are compared in Figures 11 and 12. Note that the main radiation pattern and maximum realized gain occur at the direction of $\theta = 0°$, which is difficult to measure in reality due to the antenna's structure and limited facilities. Thus, measurements in the *xoy* plane (horizontal plane) were performed to verify the design. To better understand the radiation characteristics of the antenna, the simulated 3D patterns and maximum realized gain are attached as references.

The 2D radiation patterns are plotted in the *xoy* plane at 172, 295, and 462 MHz, respectively. In the radiation pattern measurement, the E-field parallel to the horizontal plane (also known as the *antenna rotation plane*) is defined as *horizontal polarization*. Good agreements are observed for both polarizations. Simulated 3D patterns are presented. It is found that the main lobes of the radiation patterns at different frequencies are in the same direction (the direction of $\theta = 0°$), indicating that

the antenna has a stable working mode throughout the working frequency band.

The realized gain was measured in the direction of $\theta = 90°$ and $\varphi = 180°$. For different states with various water heights, the realized gain was measured and the envelope is recorded in Figure 12. Again, similar shapes are observed between simulations and measurements. As a reference, the simulated maximum realized gain, i.e., a function of the frequency, is added. The maximum gain occurs at the direction of $\theta = 0°$, which is higher than 5 dB, with good flatness across the required band.

To evaluate the performance of the antenna with a liquid control system, the water DRA integrated with both the electrical and fluid control was set up, as shown in Figure 13. Measurements were carried out and the reconfigurable process was managed by the liquid control software. Results are recorded and the envelope of $S_{11} < -10$ dB is depicted in Figure 14. It is observed that the working frequency of the antenna can be continuously tuned over a very wide frequency range with excellent impedance matching.

A comparison between the proposed design and several published designs is listed in Table 1. It is apparent that this article provides the widest tuning range across the frequency band, while the performance of our design is better than most of the previous designs in terms of its size, efficiency, and system tuning process.

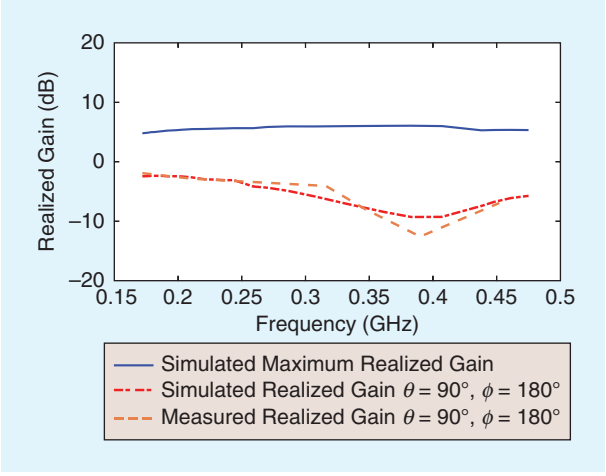

FIGURE 12. The simulated and measured realized gain comparison of the proposed antenna.

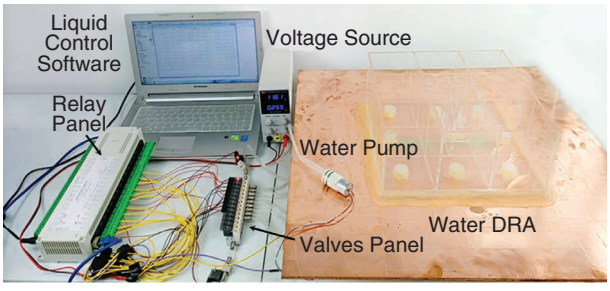

FIGURE 13. A photo of the water DRA integrated with a liquid control system.

TEMPERATURE EFFECTS ON THE PERFORMANCE OF THE PROPOSED DESIGN

The electrical properties of distilled water are a function of temperature and frequency and affect the performance of the proposed antenna. In this section, temperature effects on the electrical properties of distilled water and the performance of the proposed design are discussed.

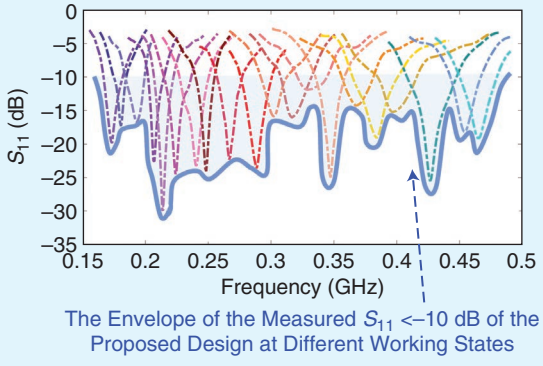

FIGURE 14. The measured S_{11} of the proposed water DRA with a liquid control system.

TABLE 1. A COMPARISON OF THE PROPOSED DESIGN AND RELATED DESIGNS.

Reference	Frequency Band (MHz)	Dimensions (mm^3)	Efficiency (%) at a Lower Bound of the Working Frequency (MHz)	Efficiency (%) at a Higher Bound of the Working Frequency (MHz)
[3]	50–100	800 × 800 × 300 (0.13λ × 0.13λ × 0.05λ @ 50 MHz)	N/A	N/A
[15]	155–400	350 × 350 × 150 (0.17λ × 0.17λ × 0.07λ @ 155 MHz)	95% at 155 (radiation efficiency)	90% at 400 (radiation efficiency)
[24]	4,660–5,650	50 × 30 × 12 (0.78λ × 0.468λ × 0.19λ @ 4,660 MHz)	64% at 4,660 (total efficiency)	81% at 5,650 (total efficiency)
This work	168–474	278 × 278 × 131 (0.155λ × 0.155λ × 0.073λ @ 168 MHz)	94.4% at 168 (total efficiency)	80% at 474 (total efficiency)

N/A: not applicable.

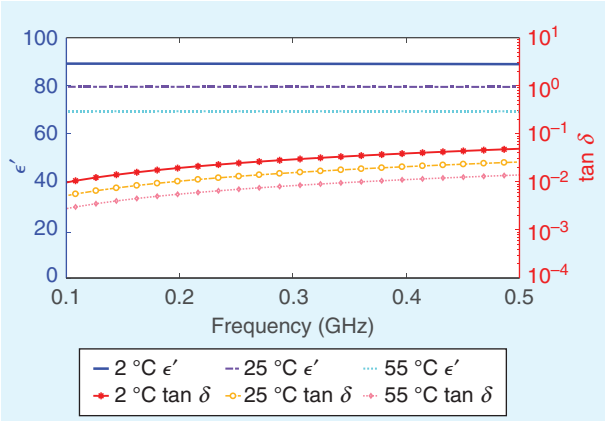

FIGURE 15. The measured relative permittivity and loss tangent of distilled water versus frequency at different temperatures.

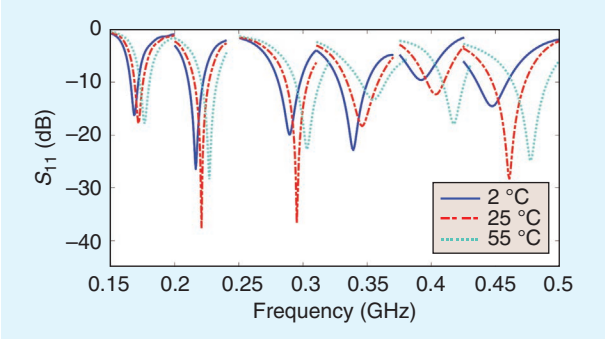

FIGURE 16. The simulated S_{11} of the proposed water DRA at different temperatures.

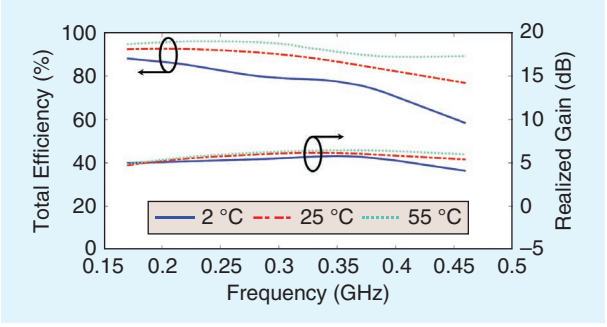

FIGURE 17. The simulated total efficiency and realized gain of the proposed water DRA at different temperatures.

At different temperatures, the distilled water was measured and the results are given in Figure 15. At a given frequency and with an increase in temperature, the relative permittivity ε' and the loss tangent $\tan\delta$ of the distilled water decrease. For a given temperature, the relative permittivity ε' is not sensitive to the frequency of interest, and the loss tangent $\tan\delta$ gradually increases with the frequency. The loss tangent of distilled water is less than 0.05 (a frequency from 0.1 to 0.5 GHz and a temperature from 2 to 65 °C), which is not significant across the band.

The S_{11}, total efficiency, and realized gain of the proposed design under different temperatures are simulated and

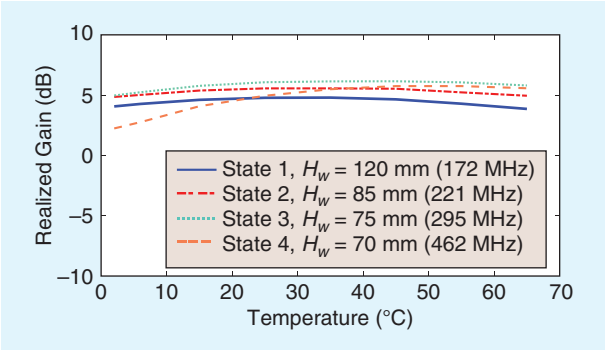

FIGURE 18. The simulated realized gain of the proposed water DRA versus temperature at different working states.

displayed in Figures 16–18, respectively. A wide frequency-tuning range can be achieved for different temperatures. The center frequency of typical states at different temperatures is slightly shifted, due to the relative permittivity variations of the distilled water. The proposed antenna's total efficiency increases with the temperature, which is mainly caused by the decrease of water loss at higher frequencies. Similar trends are also observed for the realized gain of the proposed design.

The realized gain of four typical working states versus temperature is presented. For each working state, the realized gain of the proposed design is relatively stable across a temperature range from 2 to 65 °C, indicating that the proposed antenna has a good gain response in a wide temperature range.

The distilled water will be frozen below 0 °C, thus influencing the performance of the antenna. Solutions suggested in [13], [14], and [22] use ionic liquid materials or water with a propylene glycol solution as alternative liquids, which can lower the freezing point without changing the antenna performance significantly [23].

CONCLUSIONS

In this article, a frequency-reconfigurable water antenna with a liquid control system was proposed. A liquid control system was developed. The water DRA with and without the control system was also demonstrated. Parametric studies were performed to investigate the effects of each variable so as to obtain an optimized antenna, which was fabricated and measured. The measured results agreed well with the simulated results. It was demonstrated that this antenna covered a very wide frequency-tuning range from 168 to 474 MHz (a fractional bandwidth of 95.3%), with a compact size ($278 \times 278 \times 131$ mm^3, roughly $0.155\lambda \times 0.155\lambda \times 0.073\lambda$ at 168 MHz) and high total efficiency ($> 80\%$).

The key contributions of this article were as follows:

- A high-efficiency transparent water DRA with a wide frequency-tuning range was designed. This design took full advantage of water to realize water DRAs with reconfigurable dimensions in one structure. The unique features of water in terms of high permittivity, transparency, and great design flexibility were implemented to demonstrate the antenna's excellent performance.
- A control system for liquid antennas was developed. This system managed water in an efficient way and overcame the limits of current reconfigurable water antennas. It

greatly improved the frequency-tuning efficiency of the water antenna and could be applied to large-scale water antenna designs.

This work successfully demonstrated that water antennas are good alternatives to traditional antennas in special applications, and the proposed design has great potential for VHF and UHF applications.

ACKNOWLEDGMENTS

This work was supported in part by the National Natural Science Foundation of China under grants 61601219 and 61701224 and the Nature Science Foundation of Jiangsu Province under grant BK20160804.

AUTHOR INFORMATION

Lei Xing (xinglei@nuaa.edu.cn) is a lecturer with the College of Electronic and Information Engineering, Nanjing University of Aeronautics and Astronautics, China. Her research interests include liquid antennas and antenna measurements. She is a Member of the IEEE.

Qian Xu (emxu@foxmail.com) is an associate professor with the College of Electronic and Information Engineering, Nanjing University of Aeronautics and Astronautics, China. His research interests include statistical electromagnetics and reverberation chambers. He is a Member of the IEEE.

Jiajia Zhu (emzhujiajia@foxmail.com) is currently pursuing her M.Sc. degree in microwave engineering at the College of Electronic and Information Engineering, Nanjing University of Aeronautics and Astronautics, China. Her research interests include liquid antennas and reconfigurable antennas.

Yongjiu Zhao (yj.zhao@nuaa.edu.cn) is a professor with the College of Electronic and Information Engineering, Nanjing University of Aeronautics and Astronautics, China. His research interests include antennas, microwave components, and subsystems.

Saqer Alja'afreh (eng.saqer-jaa@mutah.edu.jo) is an assistant professor with the Department of Electrical Engineering, Mu'tah University, Karak, Jordan. His research interests include dielectric resonator antennas, multiple-input, multiple-output antennas for 4G and 5G communications and microwave circuits. He is a Member of the IEEE.

Chaoyun Song (chaoyun.song@liv.ac.uk) is currently a postdoctoral research associate with the Department of Electrical Engineering and Electronics, Liverpool, United Kingdom. His research interests include liquid antennas, novel materials, wireless energy harvesting, wireless power transfers, and rectifying antennas.

Yi Huang (yi.huang@liverpool.ac.uk) is a full professor and the deputy head of the Department of Electrical Engineering and Electronics, the University of Liverpool, United Kingdom. His research interests include wireless communications, applied electromagnetics, radar, and antennas. He is a Senior Member of the IEEE.

REFERENCES

[1] S. Cheng, Z. Wu, P. Hallbjorner, K. Hjort, and A. Rydberg, "Foldable and stretchable liquid metal planar inverted cone antenna," *IEEE Trans. Antennas Propag.*, vol. 57, no. 12, pp. 3765–3771, 2009.

[2] M. Wang, M. R. Khan, M. D. Dickey, and J. J. Adams, "A compound frequency- and polarization-reconfigurable crossed dipole using multidirectional spreading of liquid metal," *IEEE Antennas Wireless Propag. Lett.*, vol. 16, pp. 79–82, 2017.

[3] S. G. O'Keefe and S. P. Kingsley, "Tunability of liquid dielectric resonator antennas," *IEEE Antennas Wireless Propag. Lett.*, vol. 6, pp. 533–536, 2007.

[4] J. Sun and K. M. Luk, "A wideband low cost and optically transparent water patch antenna with omnidirectional conical beam radiation patterns," *IEEE Trans. Antennas Propag.*, vol. 65, no. 9, pp. 4478–4485, 2017.

[5] Z. Hu, W. Wu, Z. Shen and C. Hua, "A Yagi monopole antenna made of pure water," in *Proc. IEEE AP-S Int. Symp.*, Vancouver, Canada, 2015, pp. 2241–2242.

[6] L. Xing, Y. Huang, Y. Shen, S. Alja'afreh, Q. Xu, and R. Alrawashdeh, "Further investigation on water antennas," *IET Microw., Antennas Propag.*, vol. 9, no. 8, pp. 735–741, 2015.

[7] Z. Peng et al., "Metal-loaded seawater antenna with high radiation efficiency and wideband characteristics," *IEEE Antennas Wireless Propag. Lett.*, vol. 16, pp. 1671–1674, 2017.

[8] L. Xing, Y. Huang, Q. Xu, and S. Alja'afreh, "A wideband hybrid water antenna with an F-shaped monopole," *IEEE Access*, vol. 3, pp. 1179–1187, Aug. 2015.

[9] Y. Qian and Q. Chu, "A broadband hybrid monopole-dielectric resonator water antenna," *IEEE Antennas Wireless Propag. Lett.*, vol. 16, pp. 360–363, 2017.

[10] L. Xing, Y. Huang, Q. Xu, and S. Alja'afreh, "Compact water loaded reconfigurable antenna for DVB-H applications," *Electron. Lett.*, vol. 51, no. 24, pp. 1958–1960, 2015.

[11] Z. Gong, C. Bartone, F. Yang, and J. Yao, "High-efficiency water-loaded microwave antenna in ultra-high-frequency band," *Appl. Phys. Lett.*, vol. 112, no. 11, pp. 113,501, 2018.

[12] S. H. Zainud-Deen, M. M. Madawy and H. A. Malhat, "Gain enhancement of microstrip antenna using 3D water-based metamaterial," in *Proc. JAC-ECC*, Alexandria, Egypt, 2018, pp. 25–28.

[13] C. Song, E. L. Bennett, J. Xiao, A. Alieldin, K. M. Luk, and Y. Huang, "Metasurfaced, broadband and circularly polarized liquid antennas using a simple structure," *IEEE Trans. Antennas Propag.*, vol. 67, no. 7, pp. 4907–4913, 2019.

[14] C. Song, E. L. Bennett, J. Xiao, Q. Hua, L. Xing, and Y. Huang, "Compact ultra-wideband monopole antennas using novel liquid loading materials," *IEEE Access*, vol. 7, pp. 49,039–49,047, 2019.

[15] M. Zou, Z. Shen, and J. Pan, "Frequency-reconfigurable water antenna of circular polarization," *Appl. Phys. Lett.*, vol. 108, no. 1, p. 014102, 2016.

[16] M. Wang and Q. Chu, "A wideband polarization reconfigurable dielectric resonator antenna," *IEEE Antennas Wireless Propag. Lett.*, vol. 18, no. 2, pp. 402–406, 2019.

[17] Y. Qian and Q. Chu, "A pattern-reconfigurable water-loaded MIMO antenna," *Microw. Opt. Technol. Lett.*, vol. 59, no. 7, pp. 1608–1613, 2017.

[18] S. H. Zainud-Deen, H. A. Malhat, and M. M. Abdelbary, "Reconfigurable sea-water based reflectarray antenna for UHF applications," *Wireless Pers. Commun.*, vol. 106, no. 3, pp. 1649–1657, 2019.

[19] Z. Chen and H. Wong, "Wideband glass and liquid cylindrical dielectric resonator antenna for pattern reconfigurable design," *IEEE Trans. Antennas Propag.*, vol. 65, no. 5, pp. 2157–2164, 2017.

[20] E. A. J. Marcatili, "Dielectric rectangular waveguide and directional coupler for integrated optics," *Bell Syst. Tech. J.*, vol. 48, no. 7, pp. 2071–2102, 1969.

[21] R. K. Mongia and A. Ittipiboon, "Theoretical and experimental investigations on rectangular dielectric resonator antennas," *IEEE Trans. Antennas Propag.*, vol. 45, no. 9, pp. 1348–1356, 1997.

[22] L. Xing, Y. Huang, Q. Xu, S. Alja'afreh, and T. Liu, "Complex permittivity of water-based liquids for liquid antennas," *IEEE Antennas Wireless Propag. Lett.*, vol. 15, pp. 1626–1629, 2016.

[23] L. Xing, Y. Huang, Q. Xu, S. Alja'afreh, and T. Liu, "A broadband hybrid water antenna for hand-portable applications," *IEEE Antennas Wireless Propag. Lett.*, vol. 15, pp. 174–177, 2016.

[24] Z. P. Zhong, J. J. Liang, G. L. Huang, and T. Yuan, "A 3D- printed hybrid water antenna with tunable frequency and beamwidth," *Electronics*, vol. 7, no. 10, pp. 1–13, 2018.